



Contents lists available at ScienceDirect

Journal of Rock Mechanics and Geotechnical Engineering

journal homepage: www.jrmge.cn

Full Length Article

Thermo-hydro-poro-mechanical responses of a reservoir-induced landslide tracked by high-resolution fiber optic sensing nerves

Xiao Ye^a, Hong-Hu Zhu^{a,*}, Gang Cheng^{a,b}, Hua-Fu Pei^c, Bin Shi^a, Luca Schenato^{d,e}, Alessandro Pasuto^d

^a School of Earth Sciences and Engineering, Nanjing University, Nanjing, 210023, China

^b School of Computer Science, North China Institute of Science and Technology (National Safety Training Center of Coal Mines), Beijing, 101601, China

^c State Key Lab of Coastal and Offshore Engineering, Department of Geotechnical Engineering, Dalian University of Technology, Dalian, 116024, China

^d National Research Council-Research Institute for Geo-Hydrological Protection (CNR-IRPI), Padova, 35127, Italy

^e Department of Information Engineering, University of Padova, Padova, 35131, Italy

ARTICLE INFO

Article history:

Received 15 January 2023

Received in revised form

5 March 2023

Accepted 12 April 2023

Available online 18 May 2023

Keywords:

Reservoir landslide

Thermo-hydro-poro-mechanical response

Ultra-weak fiber bragg grating (UWFBG)

subsurface evolution

Engineering geological interface

Geotechnical monitoring

ABSTRACT

Thermo-poro-mechanical responses along sliding zone/surface have been extensively studied. However, it has not been recognized that the potential contribution of other crucial engineering geological interfaces beyond the slip surface to progressive failure. Here, we aim to investigate the subsurface multiphysics of reservoir landslides under two extreme hydrologic conditions (i.e. wet and dry), particularly within sliding masses. Based on ultra-weak fiber Bragg grating (UWFBG) technology, we employ special-purpose fiber optic sensing cables that can be implanted into boreholes as “nerves of the Earth” to collect data on soil temperature, water content, pore water pressure, and strain. The Xipu landslide in the middle reach of the Three Gorges Reservoir Area in China was selected as a case study to establish a paradigm for in situ thermo-hydro-poro-mechanical monitoring. These UWFBG-based sensing cables were vertically buried in a 31 m-deep borehole at the foot of the landslide, with a resolution of 1 m except for the pressure sensor. We reported field measurements covering the period 2021 and 2022 and produced the spatiotemporal profiles throughout the borehole. Results show that wet years are more likely to motivate landslide motions than dry years. The annual thermally active layer of the landslide has a critical depth of roughly 9 m and might move downward in warmer years. The dynamic groundwater table is located at depths of 9–15 m, where the peaked strain undergoes a periodical response of leap and withdrawal to annual hydrometeorological cycles. These interface behaviors may support the interpretation of the contribution of reservoir regulation to slope stability, allowing us to correlate them to local damage events and potential global destabilization. This paper also offers a natural framework for interpreting thermo-hydro-poro-mechanical signatures from creeping reservoir bank slopes, which may form the basis for a landslide monitoring and early warning system.

© 2024 Institute of Rock and Soil Mechanics, Chinese Academy of Sciences. Production and hosting by Elsevier B.V. This is an open access article under the CC BY license (<http://creativecommons.org/licenses/by/4.0/>).

1. Introduction

The construction and operation of dams inevitably create reservoirs that can affect the stability of slopes distributed along riverbanks (Schuster, 1979; Paronuzzi et al., 2013; Chen et al., 2022). Large-scale catastrophic reservoir landslides are a potential threat to local communities and infrastructures. The hazards are mainly

related to the large-volume rock and soil debris (i.e. value of over $1 \times 10^6 \text{ m}^3$) and potential high-speed motion. Moreover, it can be amplified by the occurrence of extreme rainfall events that are showing an increasing frequency in recent years due to climatic changes (Alonso et al., 2016; Jones et al., 2021; Ye et al., 2022). Unfortunately, these geohazard events might not be expected to lessen over time, for instance, the first half of 2022 was the deadliest on record for landslides (Westra et al., 2014; Cendrero et al., 2020; Ozturk et al., 2022; Ma and Yuan, 2023).

The Vajont landslide, which occurred on October 9, 1963, was an iconic reservoir landslide event that provoked a worldwide sensation and served as a wake-up call for hazard monitoring and

* Corresponding author.

E-mail address: zh@nju.edu.cn (H.-H. Zhu).

Peer review under responsibility of Institute of Rock and Soil Mechanics, Chinese Academy of Sciences.

mitigation in the reservoir area (Müller, 1964; Veveakis et al., 2007; Paronuzzi et al., 2013). For this, a large number of researchers have made significant efforts and contributions to this issue, such as the Qiangjianping landslide in Zigui, China, 2003 (Wang et al., 2004), San Juan de Grijalva slide in Mexico, 2007 (Alcántara-Ayala and Domínguez-Morales, 2008), and Outang landslide in Fengjie, China (Yin et al., 2016). The kinematics of these events are quite different, but they have been widely classified into flow-like earth motion and sliding motion (Hung et al., 2014). The flow-like rheology is mainly related to the hydrodynamic and rock/soil properties, which is supported by power-law viscoplastic flow theory (Iverson et al., 1997; Cascini et al., 2010; Di Maio et al., 2020; Hu et al., 2020). Instead, for creeping landslides, it is usually focused on the location and evolutionary characteristics of potential sliding surfaces (Vevakis et al., 2007; Ye et al., 2022). The impacts of the cyclic filling and drawdown operation of the reservoir are twofold: triggering a seepage process, and/or inducing a stabilizing load at the submerged slide toe (Costa and Schuster, 1988; Iqbal et al., 2017). Slope stability can thus be time-dependently enhanced or worsened. Hydromechanical responses of the sliding surface (i.e. shear zone) to predisposing factors often help in understanding the landslide deformation mechanism (Finnegan et al., 2021). The temperature changes in the shear band can be linked to the confined aquifer and landslide deformation (Vevakis et al., 2007; Seguí and Vevakis, 2021), which can be further used to evaluate the stability of deep-seated landslide and predict landslide displacement. Nevertheless, there is still a gap in understanding the thermo-hydro-poro-mechanical behaviors inside sliding masses of an activated slow-moving reservoir landslide.

One of the major challenges in landslide hydrogeology is to identify the location and characterize the multi-physics of crucial underground interfaces that can evolve into a sliding surface (Zhu, 2023). Fiber optics have been widely employed to obtain accurate temperature and strain data subjected to external forces or temperature variations (Soga and Luo, 2018; Shi et al., 2021; Xu et al., 2022a). However, measuring hydraulically relevant variables is challenging but significant, as water is the main mover of earth surface process (Palmer, 2017). More recently, fiber-optic multi-physical sensing has reached a new level in groundwater monitoring, which permits us to infer subsurface hydraulic flow paths by utilizing the thermophysical effects of the material (Selker et al., 2006; Zhang and Xue, 2019; Sun et al., 2022; Ye et al., 2022). The feasibility to obtain accurate soil-water content measurements using the active-heated fiber-optic (AHFO) temperature sensing method through laboratory tests is demonstrated (Sayde et al., 2010). Encouragingly, the AHFO technique has successfully applied to field-scale monitoring of hydrology and heat transport in porous media (Read et al., 2013; Sun et al., 2021). Fiber optics has demonstrated their potential in monitoring subsurface multi-physical behavior at high resolutions (Hasler, 2022; Sidder, 2022). Nonetheless, there are few reports on field landslide monitoring of thermo-hydro-mechanical responses of sliding masses. Actually, this particular feature is crucial in understanding the seepage processes and stress states that affected the slope stability during the filling-drawdown cycles of the reservoir (Paronuzzi et al., 2013).

In this paper, we present the results of thermo-hydro-poro-mechanical responses tracked by ultra-weak fiber Bragg grating (UWFBG) array deployed at the toe of the Xinpu landslide, in the middle reach of the Three Gorges Reservoir Area. These special-purpose UWFBG-based sensing cables, acting as a “fiber optic nerve system (FONS)” of the ground (Ye et al., 2022), were vertically buried in a 31 m-deep borehole near the reservoir shoreline to collect data on soil temperature, water content, pore water

pressure, and strain. The field-scale multi-physical measurements almost covering the years 2021–2022 display the spatiotemporal profiles in wet and dry hydrologic extremes. Thermo-hydro-poro-mechanical representations with an unprecedented level of detail will contribute to providing new insights of other crucial engineering geological interfaces besides the slip surface to infer flow fluid migration and stress relief within the sliding masses.

2. Studied landslide

2.1. Site description

The study area is situated at Xinpu Village, Fengjie County, Chongqing, in the middle reach of the Three Gorges Reservoir Area in China (Fig. 1). The Xinpu landslide, almost encompassing the whole village, is located on the right bank of the mainstream of the Yangtze River. The Shengjibao landslide was monitored 15 years ago, which is the predecessor of the current Xinpu landslide (i.e. the lower part of the landslide). In October 2006, the activation of the prior Shengjibao landslide was observed when the Three Gorges Reservoir was impounded to 156 m, resulting in extensive deformation caused by the drawdown of the reservoir water level (RWL) and seasonal rainfall (Jiang et al., 2020). In response, 16 on-site surface displacement-monitoring stations were installed over the hillslope in March 2007. Since then, localized accelerated-deformation or even acute collapse occurred almost every year within and beyond the original Shengjibao area, leading to several relocations of the residents. Consequently, the boundary was redefined and renamed as the Xinpu landslide. Regrettably, the possibility of additional resettlements cannot be dismissed, as localized large deformations and devastating failure within the landslide have become increasingly severe in recent years than ever.

As shown in Figs. 2 and 3, the Xinpu landslide is a large-scale complex landslide that ranges from 90 m above sea level (a.s.l.) (toe) to 705 m a.s.l. (crown). It covers an area of 1.94 km², with a volume of 5.4×10^7 m³ and an average slope gradient of about 18°–28°. The main sliding orientation of the slide is almost 347°. The unstable slope has been divided into four blocks in accordance with the landslide style of activity, with the lower part (Blocks I and IV) being the most dominant in terms of landslide deformation. For this, the monitoring campaign has been focused on this zone. The upper and middle parts of the slide are relatively stable (Blocks II and III). Note that the slide toe is perennially submerged under the operating RWL (i.e. 145–175 m a.s.l.), making it a typical wading landslide.

Previous drilling exploration data reveal the geological structure of the Xinpu landslide. The slide mass, from top to bottom, mainly consists of gravelly silty clay (i.e. with a gravel content of 20%–40%), gravel with silty clay (i.e., with a gravel content of 60%–80%), and crushed siltstone (Fig. 7). The thicknesses of these layers vary from 3 m to 23.8 m, 1.2 m–39.4 m, and 1 m–14 m, respectively. The closer to the slope foot, the thicker the sliding accumulation, reaching 80 m at certain locations.

2.2. Downhole fiber-optic cable configurations

To investigate the multi-physical evolution within the landslide masses, a bunch of specific-purpose fiber optic cables was installed in a 31 m-deep borehole FOS3 at the toe of the Xinpu landslide to measure soil temperature, water content, pore water pressure, and strain, respectively (Figs. 2 and 3). Among them, temperature, water content, and strain sensors were encapsulated into cables at

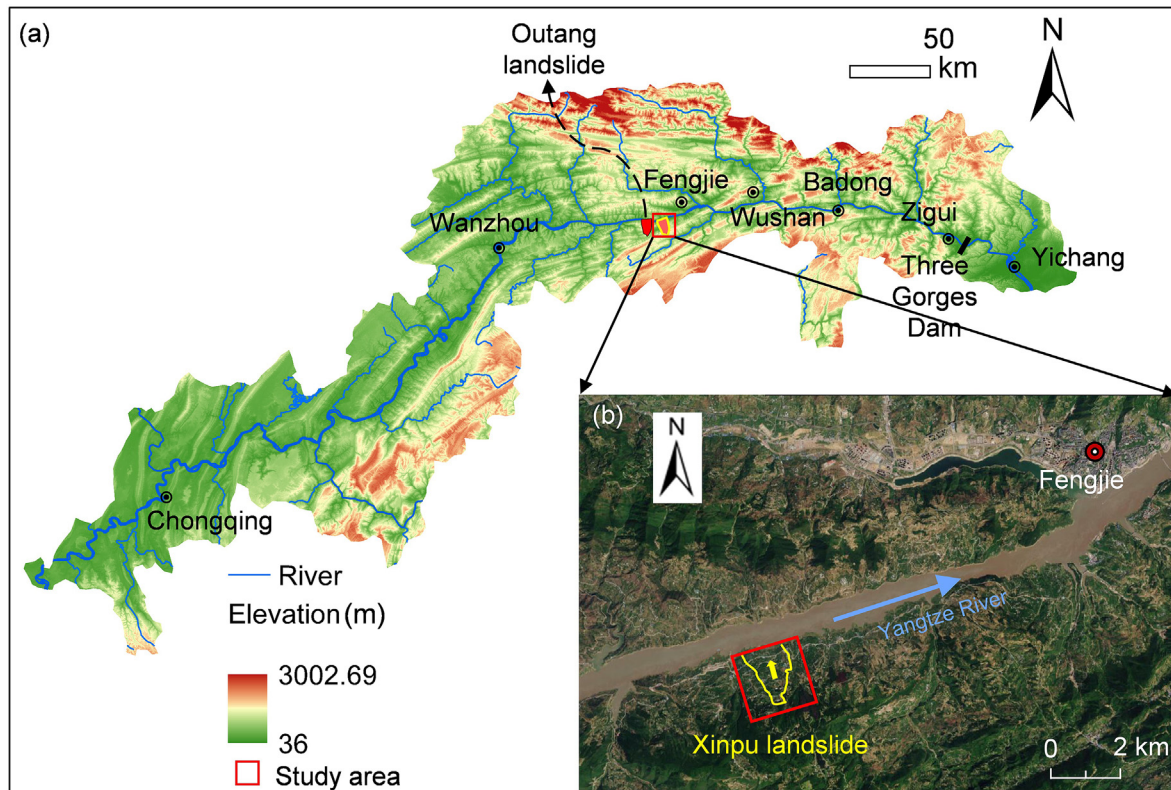


Fig. 1. Location of the study area: (a) Digital elevation model (DEM) (data from <https://srtm.csi.cgiar.org/srtmdata/>) map of the Three Gorges Reservoir area, China; and (b) Location of the Xinpu landslide bounded by yellow curve, and the sliding towards nearly north-direction.

1 m sampling intervals, forming separate sensing arrays (Fig. 4). Whereas three piezometric pressure sensors were installed in a 2 m-deep sand filter at depths of 10 m, 20 m, and 30 m down the borehole. The interrogator was in situ left in a protective box at the surface near the borehole, and the data were acquired remotely and in real time, typically with a sampling frequency of 1–60 min (Fig. 4f and g). The initial reference measurements started on February 11, 2021, which was approximately three weeks after backfilling allowing possible effects of compressional consolidation of the filling materials in the borehole to relax and therefore eliminating their effects on the results.

3. Data and methods

3.1. Principle of UWFBG

Fiber optic Bragg grating (FBG) is one of the most mature fiber optic sensing technology that has been widely employed for geo-engineering health monitoring (Kelam et al., 2016, 2022). The principle of FBG sensing technology is to create a wavelength selective mirror, by periodically changing the refractive index of the fiber core (i.e. the grating) (Ho et al., 2006). External forces, and the consequent longitudinal strain or temperature variations applied to the grating determine a reproducible shift of the central reflected wavelength of the grating (Soga and Luo, 2018). In general, the amount of wavelength shift of the central reflect wavelength encodes simultaneously the overall effects of strain and temperature.

One of the main advantages of this technology is the multiplexing capability, with tens of sensors localized in the same fiber to implement an array of daisy-chained sensors. If each FBG of such

an array has a distinct central wavelength, the entire array can be simultaneously interrogated by the so-called wavelength division multiplexing (WDM) technique, which allow addressing each FBG by its own central wavelength. However, it fails to provide a truly continuous description of strain or temperature changes because the number of sensing points (i.e. gratings) along an optical fiber is limited to some tens, depending on the bandwidth requirements of each FBG (Moyo et al., 2005). The limited number of FBGs allocable in a single fiber determines, in turn, a constraint on the spatial resolution, especially if the area to be monitored is wide. Although FBG sensing, in some cases, can provide useful and cost-effective information about global behavior, in some applications it can give only a coarse or partial representation of a specific area of the phenomena.

The UWFBG refers to as a particular FBG technology implemented by gratings with reflectivity of less than 0.01% (−40 dB). Askins et al. (1992) developed a weak-reflection FBG with reflectivity less than 2% and linewidth of about 0.1 nm, and proposed its use as a unit to form a serialized, distributed and addressable sensor array. UWFBG technology has developed over decades to make it possible to apply in various engineering scenarios (Lindner et al., 2014; Yang et al., 2016). In one of the most effective implementations, a large-scale and dense UWFBG sensor array is made up of hundreds or thousands of identical-wavelength FBGs. Given the spectral overlapping of the gratings, the time-division multiplexing (TDM) technique is utilized to enable the simultaneous measurement of numerous gratings along a single fiber, as depicted in Fig. 5. This greatly enhances the sensing capacity and offers a spatial resolution of less than 1.0 m that is well-suited to capture hydro- and geo-mechanical behavior of subsurface thin-layer

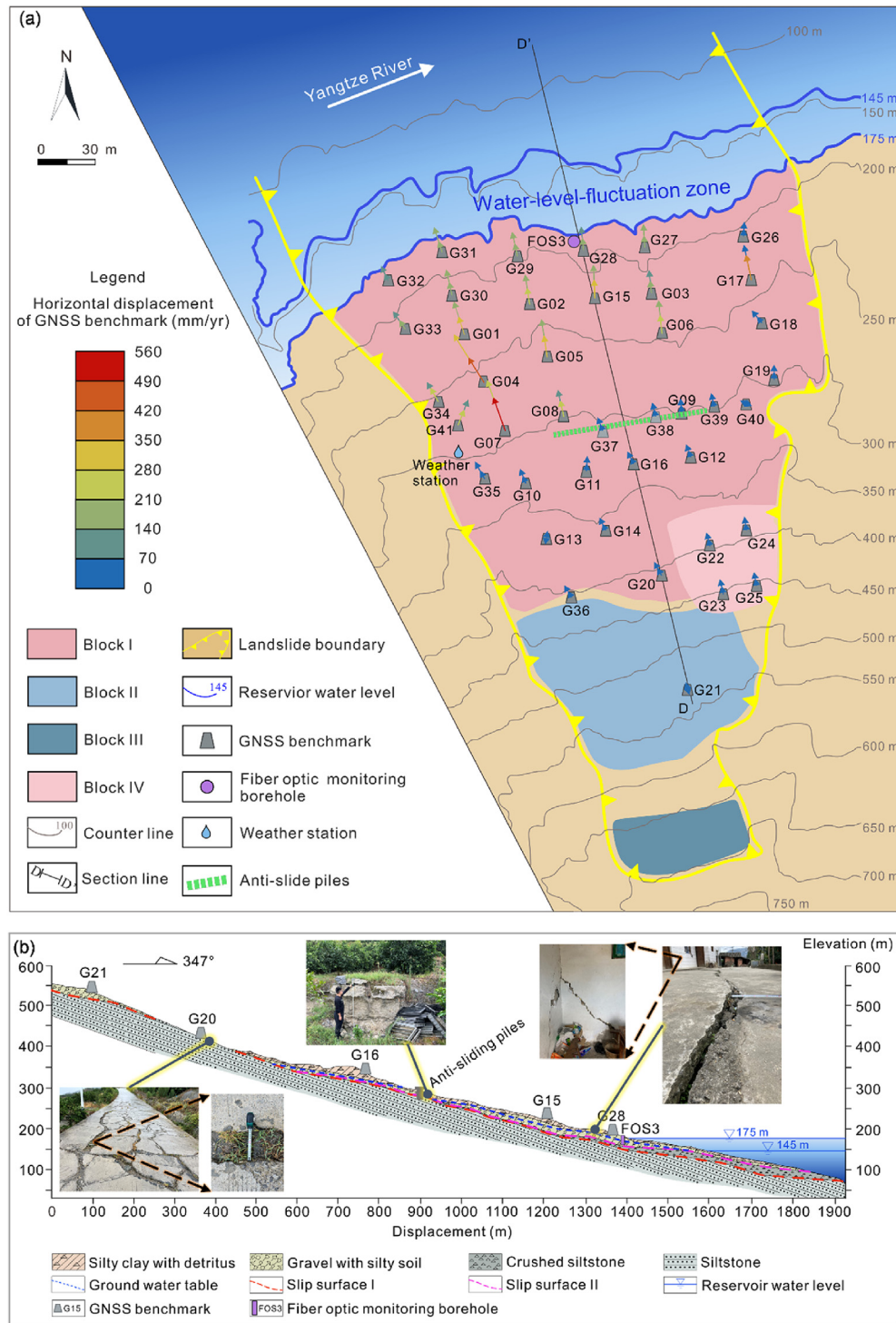


Fig. 2. Map view of the borehole FOS3 location alongside the Yangtze River in 2020 and indication of the extent of the investigated slope instability: (a) Planar map marked annual surface displacements in 2021 and 2022 using vectored arrows, and the color and orientation of the arrows indicate the magnitude and direction of landslide deformation; and (b) Geological profile D-D', together with in situ instruments and macroscopic deformation evidence including cracking of residential houses, ground subsidence fronted a line of anti-slide piles (reaching approximately 2 m), ubiquitous tension cracks onto roads with a width of up to 10–20 cm.

interfaces (Liu et al., 2021; Ye et al., 2022). With the TDM interrogation technique, each grating of the fiber can be addressed from the time difference among the arrival of reflected light passing the entire grating sequence back. Given the vertical deployment of the fiber in the borehole, it allows to probe a specific depth in the

borehole where the sensor is located. As specified above, four separated UWFBG arrays were installed, one for each of the measured parameters (i.e. temperature, water content, strain, and pore water pressure).

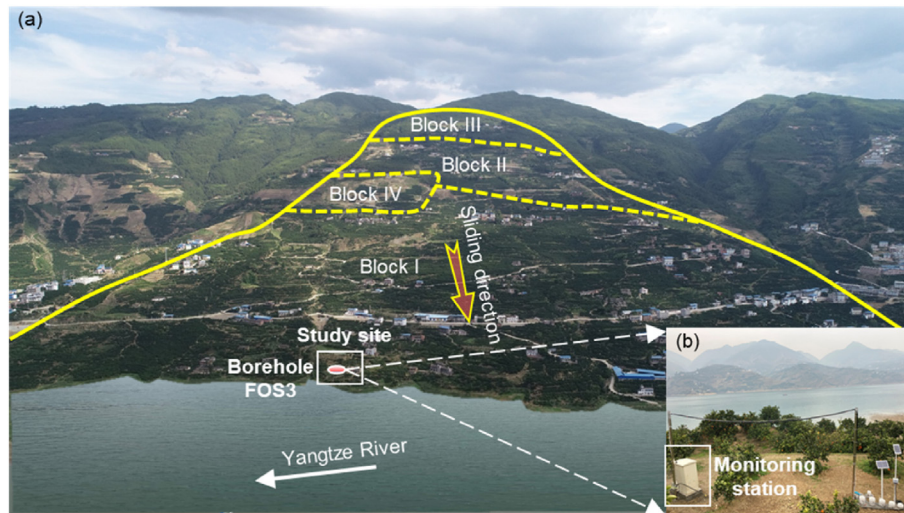


Fig. 3. Overview of the Xinpu landslide: (a) Aerial photo of the studied landslide that is zoned four blocks; and (b) Partially enlarged study site and instrumented borehole FOS3, the monitoring box is left on the surface for storing acquisition, communication and control equipment introduced residential electricity supply, rather than a solar panel.



Fig. 4. Field installation of UWFBG sensing arrays: (a) Temperature sensing cable; (b) Moisture sensing cable; (c) Strain sensing cable; (d) Pore water pressure cell; (e) Instrumented borehole to be downwards placed and backfilled; (f) Monitoring box at the top of the borehole FOS3; and (g) In situ interrogator.

By means of temperature compensation or hollow configuration between the optical fiber and sheath, strain and temperature are readily separated from each other (Zhu et al., 2017). It is noted that both the sheaths of temperature and moisture cable are highly thermally conductive, ensuring highly-sensitive temperature measurement (Fig. 4a and b). The water content measurement is performed by an actively-heated UWFBG (AH-UWFBG) moisture sensing cable, which allows for estimation of the water content from the temperature dynamics of the heated cable according to a specific temperature model (Read et al., 2013; Sun et al., 2021; Ye et al., 2022). The strain cable jacket is designed with anchor sections at an interval of 1 m to improve coupling with the soils, and the inclusion of wire ropes enhances its suitability in harsh field conditions (Fig. 4c).

3.2. Data preparation

3.2.1. Temperature, water content, pore water pressure, and strain measurements

To obtain accurate measurements, these sensors installed in the borehole need to be calibrated in advance by means of laboratory tests. The temperature or strain coefficient is determined by taking the average of the results of repeated multiple calibrations (see Fig. S1). The calibration methods can be referred to as the previous works (e.g. Liu et al., 2021; Zhang et al., 2021a; Ye et al., 2022).

To calibrate the temperature-related fiber optic cables (i.e. temperature and moisture), the cables were coiled and placed in a thermostat for gradual heating to obtain different levels of wavelength and temperature curves, which were then used to calculate

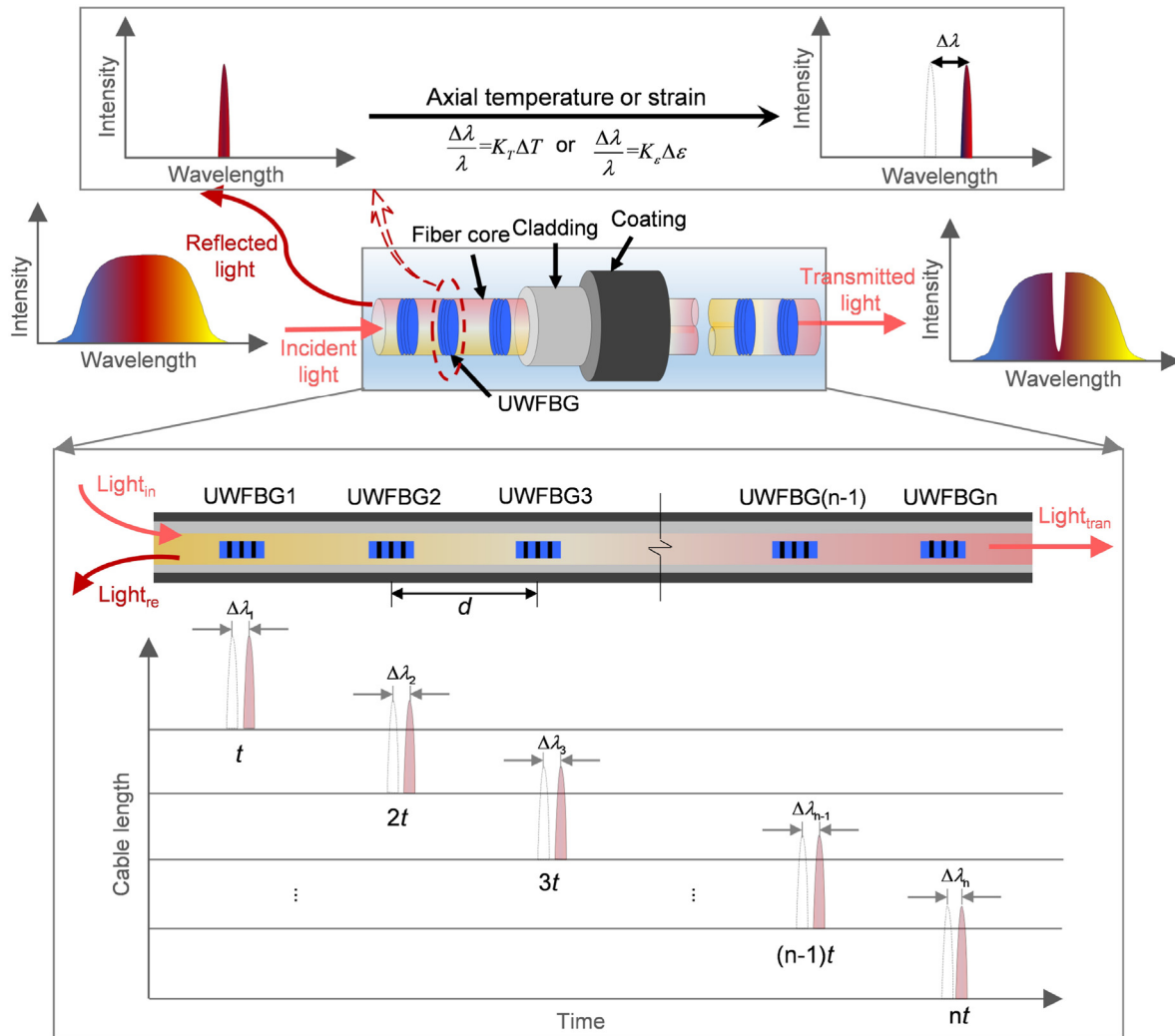


Fig. 5. Sensing principle of UWFBG array.

temperature sensitivity coefficients. Further, a remaining section of the moisture sensing cable installed in the field borehole was buried in a laboratory-scale soil column model, and the temperature increments at different water contents were determined as temperature characteristic values (i.e. temperature increments). The heating setup used in the laboratory was consistent with the field setup. Finally, the water content was quantitatively estimated by fitting the relationship between the temperature characteristic value and the volumetric soil water content.

To calibrate the pore pressure, the FBG pore pressure cell was placed inside a sealed water tank and gradually pressurized to determine the wavelength-pressure correlation. Similarly, for strain calibration, a section of the strain sensing cable was subjected to a tensile test while maintaining a constant temperature, and the strain sensitivity coefficient was obtained. According to the principle of FBG sensing, temperature, water content, pore water pressure, and strain were respectively inverted from the measured wavelengths.

3.2.2. Surface displacement

Surface displacements were measured by 41 global navigation satellite system (GNSS) benchmarks and 2 reference points distributed over the slope surface. The reference point is the iron tube placed in a stabilized area. The GNSS observations collected

during the same time period (i.e. from January 1, 2021, to November 10, 2022) as our fiber optic sensing reveal the spatiotemporal pattern of the landslide surface deformation. It provides a valuable comparison for the subsurface monitoring results (Fig. 2).

3.2.3. Reservoir water level (RWL)

The TGR was first impounded to ~135 m a.s.l. in June 2003, then to ~172 m a.s.l. in September 2008, and 175 m a.s.l. in October 2010. Since then, the RWL has been regulated to maintain a flood control level between 145 m a.s.l. and 175 m a.s.l. per year. More specifically, the reservoir level is routinely adjusted to a low level during the rainy season from May to September to mitigate the risk of flooding, and rises back to a high level during other months when precipitation is less.

3.2.4. Meteorological data

Meteorological data used in this study were collected from a weather station installed on the western part of the landslide. Daily records of precipitation and air temperature since 2021 are available, along with other climate-related variables such as wind velocity, atmospheric pressure, and ultraviolet intensity. The station can record these data every 30 min.

4. Results and analyses

In this section, we analyzed the monitoring data (February 11, 2021–November 10, 2022) to investigate the subsurface thermo-hydro-poro-mechanical behavior within the sliding masses of the lower Xinpu landslide. Note that the data were missing from June 13–28, 2021 due to the anthropogenic interruption of the system power supply.

4.1. Subsurface multi-physical evolution of sliding masses

4.1.1. Soil temperature

The full annual subsurface temperature cycle (ignoring the data gap in gray) since February 11, 2021 is reported in Fig. 6. The temperature profile, linearly interpolated, shows a depth of around 9 m of the annual thermally active layer, where the soil temperature varies in the range of 16–23 °C. Surface temperature measured by the uppermost sensor corresponded well with air temperature records, exhibiting distinct hot and cold seasons. The near-surface temperature varied in the range of 13–38 °C (Freifeld et al., 2008). In contrast, in the thermally inactive layer, variations in soil temperature were relatively sluggish, with only a magnitude of about 3 °C. Additionally, it seems to be a temperature skew at depths of 9–14 m from early April to mid-October in 2021, but the reason is, at the time being, unknown.

Fig. 7 compares the monthly mean temperature distribution in the borehole FOS3 throughout the monitoring period of 2021 and 2022, along with a stratigraphic column illustrating the material composition from the borehole core samples. It is found that the temperature fluctuation in 2022 was less than that in 2021. This might be partly explained by the progressive consolidation of the borehole backfilling which contributes to more robust temperature measurement. This is also the reason that the thermal active layer

interface has not been observed with an obvious downward shift in 2022, despite higher near-surface temperatures than those in 2021 (Luo et al., 2022). In addition, the ideal linear temperature distribution (i.e. geothermal gradient) has not been found because this borehole is not deep enough (Rybach and Pfister, 1994).

4.1.2. Water content

Fig. 8a outlines the linearly interpolated water content distribution and its evolution in the considered time-span. We observed an interface of an annual active thermo-hydraulic layer (marked in red dashed dot-dot line), which was also mostly supported by the aforementioned temperature profile. Within these depths, the atmosphere strongly interacted with shallow soils, maintaining a highly active thermo-hydraulic energy conversion, varying from 0.13 m³/m³ to 0.32 m³/m³ of the water content. More specifically, it was featuring significant rainfall infiltration and soil evaporation during the rainy season (Blight, 1997; Sun et al., 2021, 2022). In contrast, water was broadly buffered in shallow soils due to weaker evaporation during the non-rainy season. We noted the evident leaps in water content at shallow depths indicating infiltrated rainfall, such as on July 7 and August 26, 2021. Moreover, we argued that the water content within depths of 7 m was overestimated during the approximate initial three months of the monitoring campaign. This could be explained by a measurement artifact caused by the borehole construction, which would be naturally removed over time (Hugentobler et al., 2020).

Strikingly, the evolved water content profile revealed a dynamic groundwater table that fluctuated ranging from 9 m to 15 m (marked in yellow dashed dot-dot line). The groundwater level perfectly matched the RWL regulation, lagging approximately 40 d behind the filling-drawdown of the reservoir water (Prokešová et al., 2013). The groundwater levels inferred from the water content measurements were quite reasonable, since the drilling, for

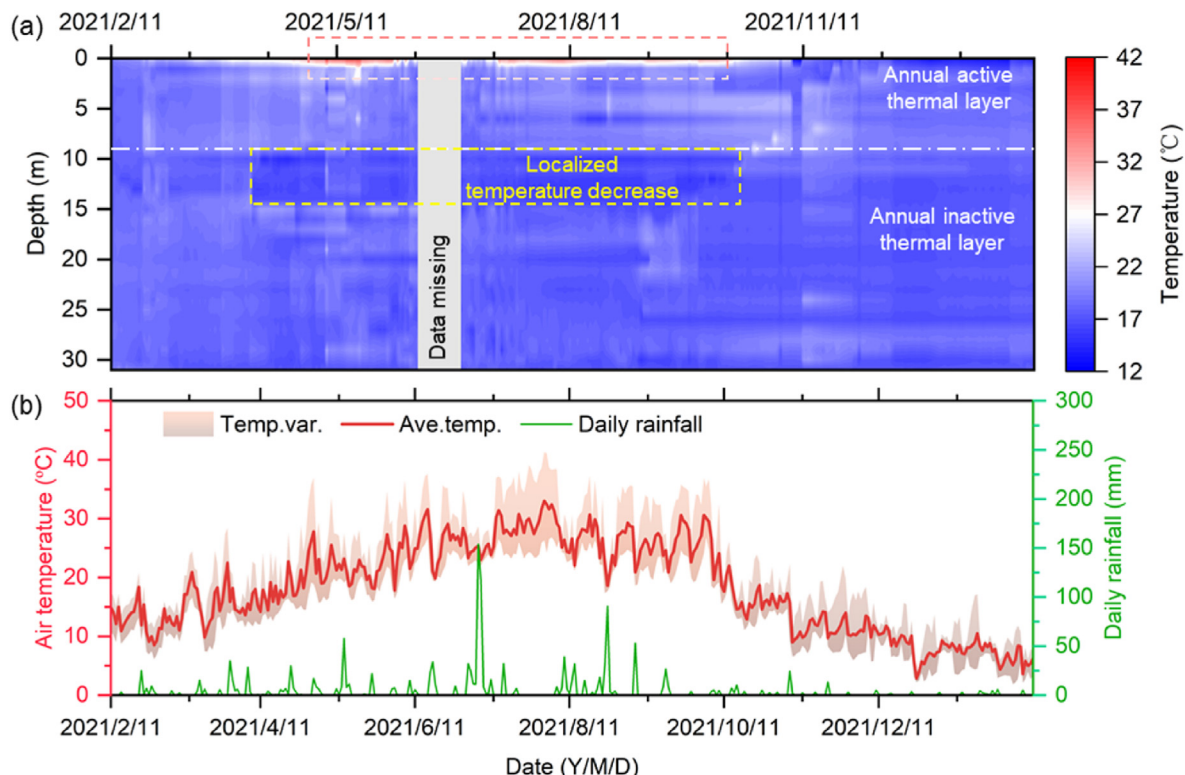


Fig. 6. Annual thermal responses to the meteorological records: (a) Soil temperature profile; and (b) Ambient temperature and rainfall events.

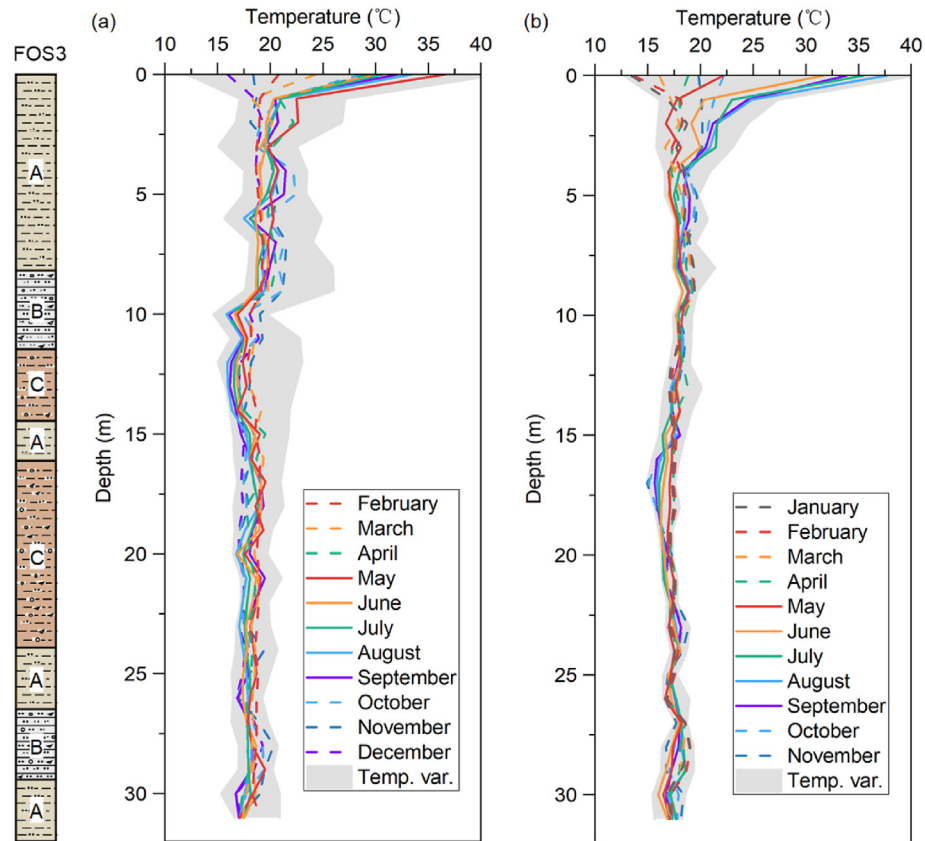


Fig. 7. Monthly mean subsurface temperature profiles in research borehole FOS3, along with the temperature range indicated in gray: (a) 2021 and (b) 2022. The left column profiles stratigraphic distribution according to the drilling core samples: A–C represent silty clay, crushed siltstone with gravel, and gravelly silty clay, respectively.

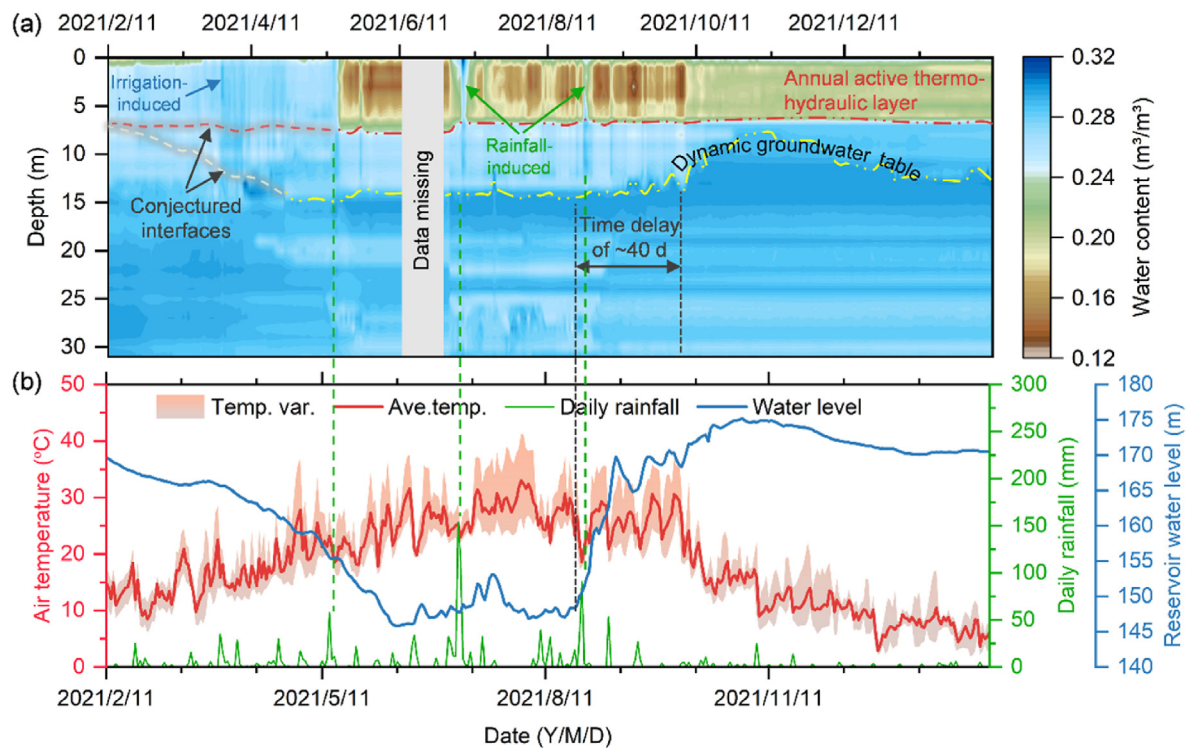


Fig. 8. Annual hydraulic responses to the hydrometeorological records: (a) Water content profile, and (b) RWL and their fluctuations.

installation of the fiber optic cables in mid-January 2021, had recorded a dive level at a depth of 13 m. The increased water content at the end of March 2021 was confirmed to be caused by agricultural irrigation lasting for several days. These findings, in turn, demonstrate the potential of the UWFBG-based water content evaluation for identifying hydrologic, meteorological, and anthropogenic activities (Froude and Petley, 2018; Xu et al., 2022b; Ye et al., 2022).

4.1.3. Pore water pressure

As shown in Fig. 9, pore water pressures measured by piezometers installed in the borehole within the landslide toe provided very different pressure values. Overall, changes in pore water pressure measured by the uppermost sensor at a depth of 10 m during the monitoring period show a good temporal correlation with the reservoir level, with slight time lagging. More specifically, the increase-decrease of pore pressure was positively correlated with the fill-drawdown of the RWL. It, however, seems that pore pressure changes did not correlate with fluctuations of reservoir water. In addition, it was not observed that some rainfall events should have caused a rapid increase in pore water pressures. This is possibly related to the fact that they were mostly short-duration and high-intensity rainfalls that almost played a role of surface runoff, and partially attributed to flat terrain and borehole top covered by concrete pier. Changes in pore pressures at deeper levels were much smaller than those at the shallower ones, likely due to the lag of pore pressure transfer in deeper soils, as well as the complexity of the stratum (Schulz et al., 2018).

4.1.4. Strain

Fig. 10a depicts the annual full-depth strain profile measured since February 11, 2021. We observed a prominent peak strain zone at depths of 11–15 m (i.e. close to the conceptualized groundwater table) with a peak strain of 2.1×10^{-3} that occurred on July 25, lasting for 45 d. It is noted that the strain peak, after the rapid rise in the reservoir level to 170 m a.s.l. on September 10, 2021, gradually decreased to 1.05×10^{-3} within about two weeks and remained largely unchanged, with fluctuations of $\pm 1 \times 10^{-4}$. It suggested that the stress concentration in this zone primarily resulted from the

agricultural irrigation event at the end of March, as well as the continued drawdown of reservoir water. The presence of smectite clay at a depth of 12 m facilitated the shrinking-swelling of weathered siltstone, which in turn impacted the cohesion and friction of the soil (Baron et al., 2004). The constant rise of reservoir water since late August increased buoyancy at the landslide foot, which contributed to enhancing the landslide stability and exhibited a strain relaxation (Ferrari et al., 2011; Tang et al., 2019).

We further compared strain profiles characterized by monthly mean values throughout the monitoring period to clarify the spatial strain distribution and inter-annual evolution (Fig. 11a). There was nearly 50% strain reduction at a depth of 13 m from August to December 2021, which was completely different from that within depths of 2.5–7.5 m (i.e. slightly increased compression strain). It suggests that the high-level reservoir water caused reversible deformation at the landslide toe. In contrast, the strain variability in 2022 is much smaller than that in 2021. One possible reason is that the overall landslide deformation in 2022 is much smaller (Fig. 2a). Furthermore, the Yangtze River Basin underwent an unprecedented extreme drought in 2022 (Ma and Yuan, 2023), which led to a delay in the regulation of RWL compared to previous years (e.g. 170 m a.s.l. on September 10, 2021, compared to 148 m a.s.l. on September 10, 2022). This is the reason that the strain contraction was not clearly observed in 2022. As mentioned earlier, such reservoir-induced reversible strain (i.e. implying reversible deformation) may be transformed into irreversible displacements during cyclic reservoir regulation, which macroscopically manifests as an increasingly flattened surface uplift at the landslide toe.

4.2. Slope kinematics and its potential controls

According to the data provided by the monitoring system, the recorded surface deformation was much larger in 2021 than that in 2022 (Fig. 12a), and this deformation was mostly concentrated in the area below the “anti-slide” piles row, thus confirming the effectiveness of such countermeasure (Zhang et al., 2023). In particular, the landslide kinematic behavior of the upper part of the unstable slope exhibits almost a constant slow deformation trend (e.g. G16, G20, G21), whereas the area below the piles shows a

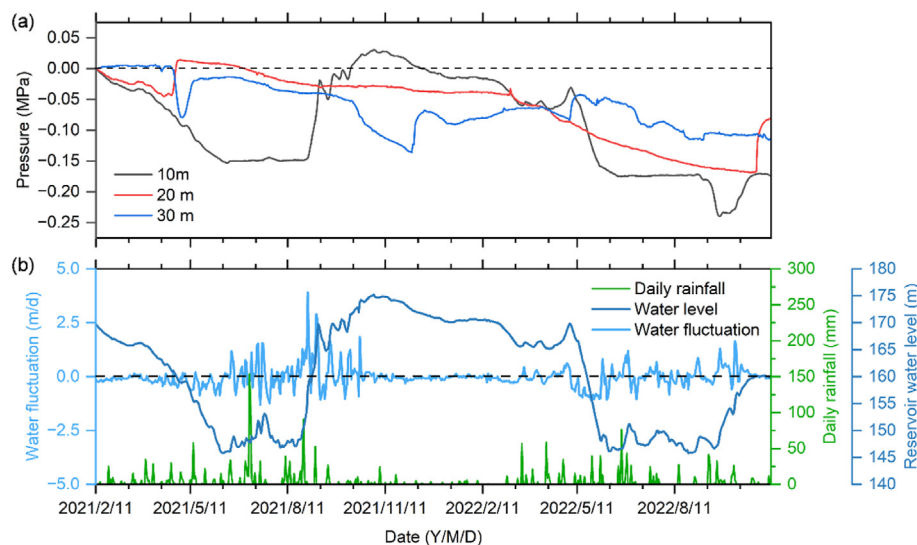


Fig. 9. Annual variations in pore water pressures at depths of interest: (a) Pore pressure versus time; and (b) Daily rainfall, RWL, and their fluctuations.

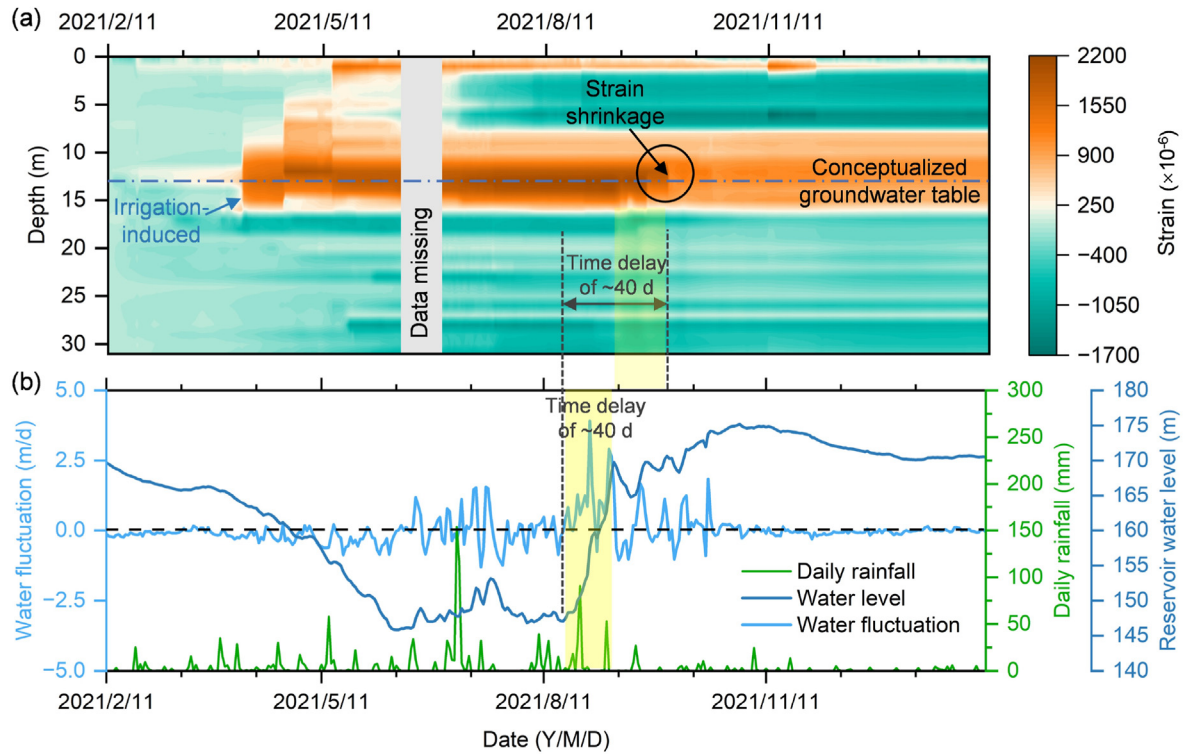


Fig. 10. Annual variations in strain: (a) Strain profile; and (b) Records of rainfall and reservoir water levels.

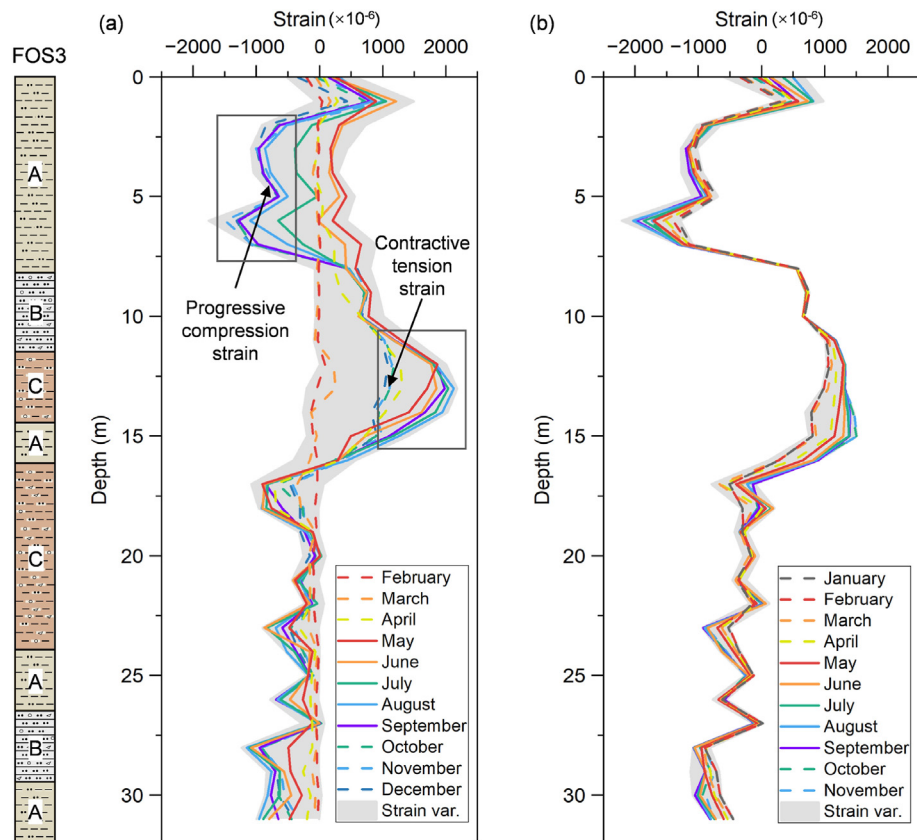


Fig. 11. Monthly mean subsurface strain profiles in borehole FOS3 in (a) 2021 and (b) 2022. The annual strain ranges are marked in gray.

typical step-like deformation pattern in response to the drawdown of reservoir level and/or concentrated rainfall (e.g. G02, G03, G28, G15). It assumes that these stepwise surface displacements were primarily governed by the constant decrease of RWL with a time lag of about 1–1.5 months; a large amount of rainfall further accelerated the deformation. The period of rapid increase of surface displacement in 2021 was prolonged due to a few high-intensity rainfall events, triggering shallow landslides especially in the lower part of the slope (Fan et al., 2020). In contrast, the slight increase of surface displacements in 2022 might be induced by the drawdown of reservoir levels. The entire landslide exhibited an insignificant displacement trend, even within the most active lower part of the landslide (Fig. 2a). The landslide movement behavior characterized by surface displacement at the slide toe and borehole strain is consistent (see Figs. 10–12). In addition, the extreme drought also forced a change in water level regulation for the 2022 flood season, representing an extended low water period (i.e. 150 m a.s.l.) of at least 1 month. Preliminary results suggest that the deformation mechanism of the Xinpu landslide driven by the drawdown of RWL and rainfall is similar to the Shuping landslide, Taping landslide, and Majiagou landslide (Song et al., 2018; Zhang et al., 2021b, 2021c).

5. Discussion

5.1. Thermo-hydro-poro-mechanical behavior within sliding masses

Temperature, water content, pore water pressure, and strain sensing arrays co-located in a single borehole reveal the effects of annual hydrometeorological cycles on the transient subsurface thermo-hydro-poro-mechanical regime. The annual thermally active layer of the landslide is roughly 9 m thick, which may appropriately shift downward with a warming climate. The water content measurement opens new perspectives for groundwater monitoring, showing an excellent correlation of peak water content evolution with reservoir level regulation and documenting that hydraulic activity within the sliding mass lags behind reservoir levels significantly. The data so far gathered indicate that seasonal pore pressure changes are primarily regulated by reservoir levels rather than rainfall and snowmelt events. The strain sensing arrays allow us to characterize the cumulative deformation reflecting the whole landslide activity, especially at its toe. The data presented confirm that the wet years are more likely to result in substantial deformation (or damage) than dry years (Zscheischler et al., 2018;

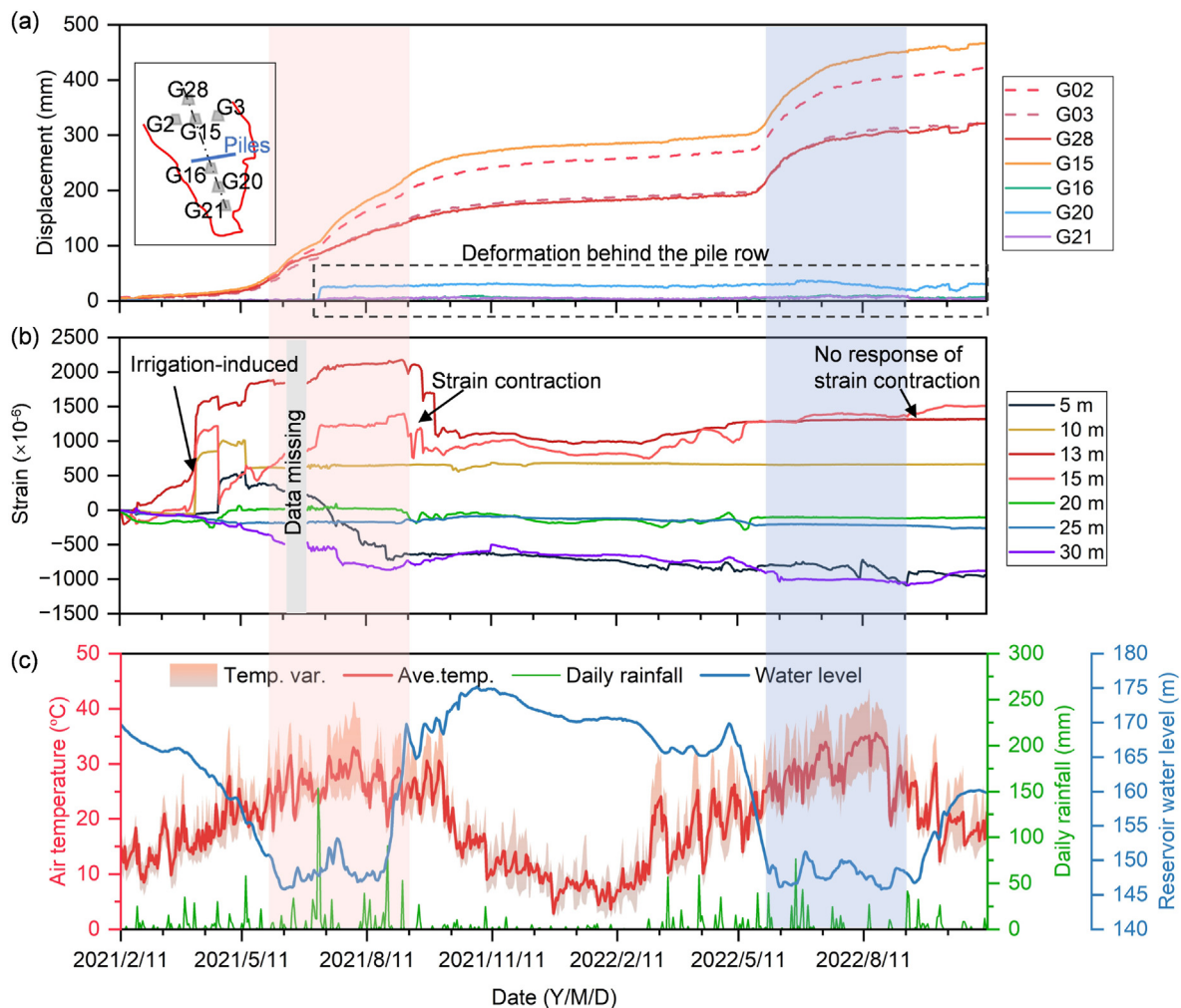


Fig. 12. Surface and subsurface kinematics linked to hydrometeorological factors: (a) Lateral surface displacements; (b) Strain time series at depths of interest; and (c) hydro-meteorological records. The flood season in 2021 and 2022 are marked by red and blue shaded areas, respectively.

De Luca et al., 2020). These potential drivers such as rapid draw-down in reservoir levels, intense storms, or extreme temperatures, often act simultaneously (Tichavský et al., 2019; Kaffle et al., 2022). The measured strain during these events usually involves irreversible and reversible components that cannot be ignored. The former is permanent damage at crucial engineering geological interfaces within the landslide driven by hydrometeorological factors, whereas the latter may be related to annual reservoir level fluctuations (Hugentobler et al., 2020).

To date, it has been challenging to distinguish the irreversible portion from the deformation associated with progressive rock damage in a relatively short monitoring time series. Nevertheless, the aim of this paper is to provide a natural framework for interpreting the thermo-hydro-poro-mechanical responses of the creeping reservoir slide, with a specific focus on the sliding mass. Here we report a preliminary study based on the monitoring results and analyses spanning almost two years. We anticipate that continued monitoring over multiple annual cycles will allow us to develop an integrated framework for multi-physical monitoring and multi-level early warning of landslide hazards (Ye et al., 2022).

5.2. Implications for understanding landslide kinematics

As illustrated in Fig. 13, in a landslide, there are often various engineering geological interfaces that involve migration of three-phase media, transformation of state and progressive changes in physical and mechanical properties, such as base-cover interface, local weak surface, interface between fractured rock and clay, diving surface and infiltration front (Zhu, 2023). These interfaces

sometimes play a controlling role in the process of gestation, development and occurrence of geological hazards. In particular, the first three are often recognized as potential sliding surfaces, where remarkable thermo-hydro-poro-mechanical changes could occur prior to landslide initiation, and macroscopically manifest as large deformations (Hu et al., 2020; Seguí and Veveakis, 2021; Scaringi and Loche, 2022). The sliding surfaces and other crucial engineering geological interfaces between bedrock and earth surface may provide inspiring information related to landslide evolution processes (Zhu, 2023). For instance, due to the morphological changes related to landslide activity, the slip surface near the slide toe is usually quite deep, but it provides an opportunity to investigate multi-physics of the interfaces between the layers of accumulated materials. Here we report inter-annual monitoring results of thermo-hydro-mechanical responses on the dynamic groundwater interface, as one of the crucial engineering geological interfaces, which reveals the evolution of the time-varying and time-delay water content, as well as the strain accumulation and withdrawal. These interface behaviors can support the interpretation of the contribution mechanism of the filling-drawdown of reservoir water on slope stability, allowing us to link them to local failure events and landslide kinematics (Paronuzzi et al., 2013; Tang et al., 2019).

The strain measurements allow some possible mechanisms to be better understood and it seems that the rate of strain accumulation may exacerbate during wet spells after a dry spell (Tichavský et al., 2019). The combined effect of extreme temperatures and rainfall has been correlated to landslide activity due to the shrinking-swelling effects of clay-rich materials, although the

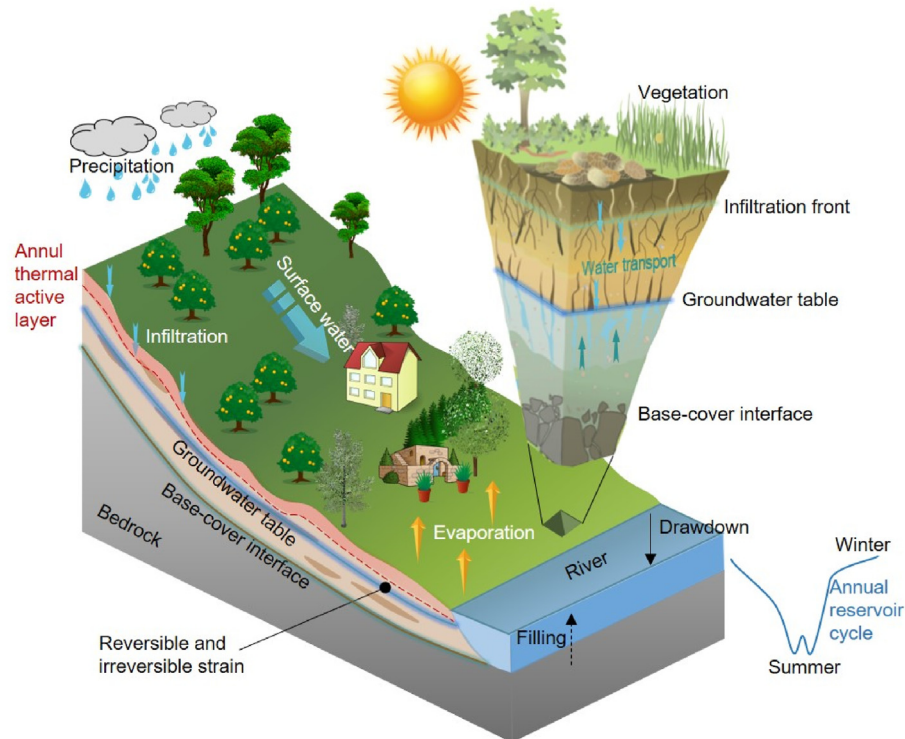


Fig. 13. Illustration of crucial engineering geological interfaces in a reservoir landslide subjected to different hydrometeorological conditions. The schematic cross-section conceptually cuts through our borehole location (FOS3), revealing annual thermal active layer, base-cover interface, as well as dynamic groundwater interface that could evolve into a potential sliding surface.

entire landslide kinematics tends to be quasi-steady state during dry spells (Lehmann and Or, 2012; Bennett et al., 2016). The “forcing” of the hydrologic cycle, that is the increase of frequency of precipitation extremes following extreme high temperatures, is likely to amplify the magnitude of sliding events (Cohen-Waeber et al., 2018; De Luca et al., 2020). We hypothesize that the transition from a quasi-stable slope to a failing landslide is a long-term and continuous process. Therefore, the preliminary findings of this paper will be critically reviewed in future studies based on our continuously updated monitoring dataset.

5.3. Applicability and limitations of UWFBG sensing nerves

Compared to the mature FBG and DFOS technologies, UWFBG allows near real-time acquisition of large amounts of multi-physical data along the fiber optic nerves with high spatial resolution such as temperature, water content, and strain (see Table S1). Specifically, the sensing elements on a single fiber optic nerve can reach over a thousand at an interval of 1 m, which is far less than FBG with comparable measurement accuracy, despite that both of them can collect data remotely and in real time. UWFBG also significantly outperforms DFOS in terms of automatization and integration of monitoring system (Zeni et al., 2015; Shi et al., 2021). Therefore, UWFBG technique is suitable for deep-seated landslides or rockslides, especially for discrimination of critical engineering geological interface (Zhu, 2023).

A major limitation so far is that only a few pore water pressure cells can be placed in a borehole with a diameter of 110 mm, given that each pressure cell contains a pie-shaped permeable stones with a diameter of 50 mm. In this aspect, unlike temperature, moisture and strain, we can only acquire depth-specific pore water pressures. Therefore, the determination of the installation depth of the pore pressure cell is challengeable and requires prior knowledge of the formation conditions. In other words, deploying such multi-physical boreholes in critical deformation areas at the lower, middle, and upper parts of the landslide could provide a possibility of understanding the subsurface thermo-hydro-poro-mechanical evolution processes of global large-scale landslides.

6. Conclusions

The present paper describes a multi-physical dataset collected from a novel borehole-based high-resolution fiber optic nerve sensing system using UWFBG technology. The system was installed to continuously record changes in below-ground soil temperature, water content, pore water pressure, and strain with a resolution of 1 m at the toe of the Xinpu landslide in the Three Gorges Reservoir Area, China, to investigate thermo-hydro-poro-mechanical responses of the unstable processes subject to periodical reservoir regulation and seasonal weather events. Here we report a preliminary study that involves monitoring data covering two recent flood periods, and the following conclusions can be drawn:

- (1) The annual thermally active layer of the landslide had a critical depth of about 9 m and might appropriately move downward in warmer years. The spatio-temporal evolution of the soil water content revealed a dynamic groundwater table fluctuating from 9 m to 15 m with a time lag of about 40 d with respect of the RWL variations.
- (2) Unlike the sluggish water pressure variation in the deep layers, the pore water pressure in the shallow layer at a depth

of 10 m showed a close connection with the filling-drawdown of the RWL.

- (3) The peak strain along the borehole profile occurred roughly at a depth of 13 m and experienced a periodical tension and relaxation to annual hydrometeorological cycles. The magnitude of such strain variations was regulated by wet and dry hydrological extremes. As expected, wet years tend to cause much larger strain accumulation, triggering more significant landslide displacements, than dry years.

Declaration of competing interest

The authors declare that they have no known competing financial interests or personal relationships that could have appeared to influence the work reported in this paper.

Acknowledgments

We acknowledge the funding support from the National Science Fund for Distinguished Young Scholars of National Natural Science Foundation of China (Grant No. 42225702) and the National Natural Science Foundation of China (Grant No. 42077235). Special thanks go to the Institute of Exploration Technology, China Geological Survey, Chengdu, China, for providing geological information of the study area. We also appreciate Xing Zheng, Jia Wang and Bing Wu in Nanjing University for their help in data processing and analyses. The first author particularly thanks Dr. Yu-Zhou Hou in 3rd Construction Co., Ltd. of China Construction 5th Engineering Bureau for his insightful comments to result analyses.

Appendix A. Supplementary data

Supplementary data to this article can be found online at <https://doi.org/10.1016/j.jrmge.2023.04.004>.

References

- Alcántara-Ayala, I., Domínguez-Morales, L., 2008. The San Juan de Grijalva catastrophic landslide, Chiapas, Mexico: lessons learnt. Tokyo, Japan. In: Sassa, K., Canuti, P. (Eds.), *Proceedings of the 1st World Landslide Forum*, pp. 96–99 (Berlin, Germany).
- Alonso, E.E., Zervos, A., Pinyol, N.M., 2016. Thermo-poro-mechanical analysis of landslides: from creeping behaviour to catastrophic failure. *Geotechnique* 66 (3), 202–219.
- Askins, C.G., Tsai, T.E., Williams, G.M., Putnam, M.A., Friebele, E.J., 1992. Fiber Bragg reflectors prepared by a single excimer pulse. *Opt. Lett.* 17 (11), 833–835.
- Baroň, I., Čilek, V., Krejčí, O., Melichar, R., Hubatka, F., 2004. Structure and dynamics of deep-seated slope failures in the magura flysch nappe, outer western carpathians (Czech republic). *Nat. Hazard Earth Sys* 4 (4), 549–562.
- Bennett, G.L., Roering, J.J., Mackey, B.H., Handwerger, A.L., Schmidt, D.A., Guillod, B.P., 2016. Historic drought puts the brakes on earthflows in Northern California. *Geophys. Res. Lett.* 43, 5725–5731.
- Blight, G.E., 1997. Interactions between the atmosphere and the earth. *Geotechnique* 47 (4), 715–767.
- Cascini, L., Cuomo, S., Pastor, M., Sorbino, G., 2010. Modeling of rainfall-induced shallow landslides of the flow-type. *J. Geotech. Geoenviron. Eng.* 1 (1), 85–98.
- Cendrero, A., Forte, L.M., Remondo, J., Cuesta-Albertos, J.A., 2020. Anthropocene geomorphic change. Climate or human activities? *Earth's Future* 8, e2019EF001305.
- Chen, M.L., Yang, X.G., Zhou, J.W., 2022. Spatial distribution and failure mechanism of water-induced landslides in the reservoir areas of Southwest China. *J. Rock Mech. Geotech. Eng.* 15 (2), 442–456.
- Cohen-Waeber, J., Bürgmann, R., Chaussard, E., Giannico, C., Ferretti, A., 2018. Spatiotemporal patterns of precipitation-modulated landslide deformation from independent component analysis of InSAR time series. *Geophys. Res. Lett.* 45, 1878–1887.
- Costa, J.E., Schuster, R.L., 1988. The formation and failure of natural dams. *Geol. Soc. Am. Bull.* 100 (7), 1054e1068.

- De Luca, P., Messori, G., Wilby, R.L., Mazzoleni, M., Di Baldassarre, G., 2020. Concurrent wet and dry hydrological extremes at the global scale. *Earth Syst. Dynam.* 11, 251–266.
- Di Maio, R., De Paola, C., Forte, G., Piegari, E., Pirone, M., Santo, A., Urciuoli, G., 2020. An integrated geological, geotechnical and geophysical approach to identify predisposing factors for landslide occurrence. *Eng. Geol.* 267, 105473.
- Fan, L.F., Lehmann, P., Zheng, C.M., Or, D., 2020. Rainfall intensity temporal patterns affect shallow landslide triggering and hazard evolution. *Geophys. Res. Lett.* 47, e2019GL085994.
- Ferrari, A., Ledesma, A., González, D.A., Corominas, J., 2011. Effects of the foot evolution on the behaviour of slow-moving landslides. *Eng. Geol.* 117, 217–218.
- Finnegan, N.J., Perkins, J.P., Nereson, A.L., Handwerger, A.L., 2021. Unsaturated flow processes and the onset of seasonal deformation in slow-moving landslides. *J. Geophys. Res.: Earth Surf.* 126, e2020JF005758.
- Freifeld, B.M., Finsterle, S., Onstott, T.C., Toole, P., Pratt, L.M., 2008. Ground surface temperature reconstructions: using in situ estimates for thermal conductivity acquired with a fiber-optic distributed thermal perturbation sensor. *Geophys. Res. Lett.* 35, L14309.
- Froude, M.J., Petley, D.N., 2018. Global fatal landslide occurrence from 2004 to 2016. *Nat. Hazards Earth Syst. Sci.* 18, 2161–2181.
- Hasler, C., 2022. Reaching new levels in groundwater monitoring. *Eos* 103. <https://doi.org/10.1029/2022EO220517>.
- Ho, Y.T., Huang, A.B., Lee, J.T., 2006. Development of a fibre Bragg grating sensed ground movement monitoring system. *Meas. Sci. Technol.* 17 (7), 1733–1740.
- Hu, X., Bürgmann, R., Schulz, W.H., Fielding, E.J., 2020. Four-dimensional surface motions of the Slumgullion landslide and quantification of hydrometeorological forcing. *Nat. Commun.* 11, 2792.
- Hugentobler, M., Loew, S., Aaron, J., Roques, C., Oestreich, N., 2020. Borehole monitoring of thermo-hydro-mechanical rock slope processes adjacent to an actively retreating glacier. *Geomorphology* 362, 107190.
- Hung, O., Leroueil, S., Picarelli, L., 2014. The Varnes classification of landslide types, an update. *Landslides* 11 (2), 167–194.
- Iqbal, J., Tu, X.B., Xu, L., 2017. Landslide hazards in reservoir areas: case study of xiangjiaba reservoir, southwest China. *Nat. Hazards Rev.* 18 (4), 04017009.
- Iverson, R.M., Reid, M.E., Lahusen, R.G., 1997. Debris-flow mobilization from landslides. *Annu. Rev. Earth Planet. Sci.* 25, 85–138.
- Jiang, H.W., Li, Y.Y., Zhou, C., Hong, H.Y., Glade, T., Yin, K.L., 2020. Landslide displacement prediction combining LSTM and SVR algorithms: a case study of Shengjibao Landslide from the Three Gorges Reservoir area. *Appl. Sci.* 10, 7830.
- Jones, J.N., Boulton, S.J., Bennett, G.L., Stokes, M., Whitworth, M.R.Z., 2021. Temporal variations in landslide distributions following extreme events: implications for landslide susceptibility modeling. *J. Geophys. Res.: Earth Surf.* 126, e2021JF006067.
- Kafle, L., Xu, W.J., Zeng, S.Y., Nagel, T., 2022. A numerical investigation of slope stability influenced by the combined effects of reservoir water level fluctuations and precipitation: a case study of the Bianjiazhai landslide in China. *Eng. Geol.* 297, 106508.
- Kelam, A.A., Akgün, H., Koçkar, M.K., 2022. Application of an optical fiber-based system for mass movement monitoring. *Environ. Earth Sci.* 81 (5), 1–18.
- Kelam, A.A., Koçkar, M.K., Akgün, H., 2016. Utilization of optical fiber system for mass movement monitoring. *Disaster Science and Engineering* 2 (1), 19–24.
- Lehmann, P., Or, D., 2012. Hydromechanical triggering of landslides: from progressive local failures to mass release. *Water Resour. Res.* 48, W03535.
- Lindner, E., Hartung, A., Chojetzki, D.H.C., Chojetzki, C., Schuster, K., Bierlich, J., Rothardt, M., 2014. Trends and future of fiber Bragg grating sensing technologies: tailored draw tower gratings (DTGs). *Proc. SPIE* 9141, 91410X.
- Liu, S.P., Shi, B., Gu, K., Zhang, C.C., He, J.H., Wu, J.H., Wei, G.Q., 2021. Fiber-optic wireless sensor network using ultra-weak fiber Bragg gratings for vertical subsurface deformation monitoring. *Nat. Hazards* 109, 2557–2573.
- Luo, M., Lau, N.C., Liu, Z., Wu, S., Wang, X., 2022. An observational investigation of spatiotemporally contiguous heatwaves in China from a 3D perspective. *Geophys. Res. Lett.* 49, e2022GL097714.
- Ma, F., Yuan, X., 2023. When will the unprecedented 2022 summer heat waves in Yangtze River basin become normal in a warming climate? *Geophys. Res. Lett.* 50, e2022GL101946.
- Moyo, P., Brownjohn, J.M.W., Suresh, R., Tjin, S.C., 2005. Development of fiber Bragg grating sensors for monitoring civil infrastructure. *Eng. Struct.* 27 (12), 1828–1834.
- Müller, L., 1964. The rock slide in the Vajont Valley. *Rock Mech. Eng. Geol.* 2 (3–4), 148–212.
- Ozturk, U., Bozzolan, E., Holcombe, E.A., Shukla, R., Pianosi, F., Wagoner, T., 2022. How climate change and unplanned urban sprawl bring more landslides. *Nature* 608, 262–265.
- Palmer, J., 2017. Creeping earth could hold secret to deadly landslides. *Nature* 548, 384–386.
- Paronuzzi, P., Rigo, E., Bolla, A., 2013. Influence of filling-drawdown cycles of the Vajont reservoir on Mt. Toc slope stability. *Geomorphology* 191 (1–2), 75–93.
- Prokešová, R., Medvedová, A., Táborík, P., Snopková, Z., 2013. Towards hydrological triggering mechanisms of large deep-seated landslides. *Landslides* 10, 239–254.
- Read, T., Bour, O., Bense, V., Le Borgne, T., Goderniaux, P., Klepikova, M.V., Hochreutener, R., Lavenant, N., Boschero, V., 2013. Characterizing groundwater flow and heat transport in fractured rock using fiber-optic distributed temperature sensing. *Geophys. Res. Lett.* 40, 2055–2059.
- Rybach, L., Pfister, M., 1994. Temperature predictions and predictive temperatures in deep tunnels. *Rock Mech. Rock Eng.* 27 (2), 77–88.
- Sayde, C., Gregory, C., Gil-Rodríguez, M., Tuffillaro, N., Tyler, S., van de Giesen, N., Hochreutener, R., Lavenant, N., Boschero, V., 2010. Feasibility of soil moisture monitoring with heated fiber optics. *Water Resour. Res.* 46, W06201.
- Scaringi, G., Loche, M., 2022. A thermo-hydro-mechanical approach to soil slope stability under climate change. *Geomorphology* 401, 108108.
- Schulz, W.H., Smith, J.B., Wang, G., Jiang, Y., Roering, J.J., 2018. Clayey landslide initiation and acceleration strongly modulated by soil swelling. *Geophys. Res. Lett.* 45 (4), 1888–1896.
- Schuster, R.L., 1979. Reservoir-induced landslides. *Bull. Int. Assoc. Eng. Geol.* 20, 8–15.
- Seguí, C., Veveakis, M., 2021. Continuous assessment of landslides by measuring their basal temperature. *Landslides* 18, 3953–3961.
- Selker, J., van de Giesen, N., Westhoff, M., Luxemburg, W., Parlange, M.B., 2006. Fiber optics opens window on stream dynamics. *Geophys. Res. Lett.* 33 (24), L24401.
- Shi, B., Zhang, D., Zhu, H.H., Zhang, C.C., Gu, K., Sang, H.W., Han, H.M., Sun, M.Y., Liu, J., 2021. DFOS applications to geo-engineering monitoring. *Photonic Sens* 11, 158–186.
- Sidder, A., 2022. Fiber optics open new frontier for landslide monitoring. *Eos* 103. <https://doi.org/10.1029/2022EO220373>.
- Soga, K., Luo, L., 2018. Distributed fiber optics sensors for civil engineering infrastructure sensing. *J. Struct. Integr. Main.* 3 (1), 1–21.
- Song, K., Wang, F.W., Yi, Q.L., Lu, S.Q., 2018. Landslide deformation behavior influenced by water level fluctuations of the Three Gorges Reservoir (China). *Eng. Geol.* 247, 58–68.
- Sun, M.Y., Shi, B., Zhang, C.C., Liu, J., Guo, J.Y., Zheng, X., Wang, Y.Q., Wei, G.Q., 2022. Quantifying the spatio-temporal variability of total water content in seasonally frozen soil using actively heated fiber Bragg grating sensing. *J. Hydrol.* 606, 127386.
- Sun, M.Y., Shi, B., Zhang, C.C., Zheng, X., Guo, J.Y., Wang, Y.Q., He, M.N., Liu, J., 2021. Quasi-distributed fiber-optic in-situ monitoring technology for large-scale measurement of soil water content and its application. *Eng. Geol.* 294, 106373.
- Tang, H.M., Wasowski, J., Juang, C.H., 2019. Geohazards in the Three Gorges Reservoir area, China—Lessons learned from decades of research. *Eng. Geol.* 261, 105267.
- Tichavský, R., Ballesteros-Cánovas, J.A., Šilhán, K., Tolasz, R., Stoffel, M., 2019. Dry spells and extreme precipitation are the main trigger of landslides in Central Europe. *Sci. Rep.* 9, 14560.
- Veveakis, E., Vardoulakis, I., Di Toro, G., 2007. Thermoporomechanics of creeping landslides: the 1963 Vaiont slide, northern Italy. *J. Geophys. Res.* 112, F03026.
- Wang, F.W., Zhang, Y.M., Huo, Z.T., Matsumoto, T., Huang, B.L., 2004. The July 14, 2003 qianjiangping landslide, three Gorges reservoir, China. *Landslides* 1, 157–162.
- Westra, S., Fowler, H.J., Evans, J.P., Alexander, L.V., Berg, P., Johnson, F., Kendon, E.J., Lenderink, G., Roberts, N.M., 2014. Future changes to the intensity and frequency of short-duration extreme rainfall. *Rev. Geophys.* 52, 522–555.
- Xu, J.J., Tang, C.S., Cheng, Q., Vahedifar, F., Liu, B., Shi, B., 2022a. Monitoring and early detection of soil desiccation cracking using distributed fibre optical sensing. *Geotechnique*. <https://doi.org/10.1680/jgeot.21.00397>.
- Xu, Y.K., Lu, Z., Leshchinsky, B., 2022b. Kinematics of irrigation-induced landslides in a Washington desert: impacts of basal geometry. *Geophys. Res. Lett.* 127 (2), e2021JF006355.
- Yang, M.H., Bai, W., Guo, H.Y., Wen, H.Q., Yu, H.H., Jiang, D.S., 2016. Huge capacity fiber-optic sensing network based on ultra-weak draw tower gratings. *Photonic Sens* 6 (1), 26–41.
- Ye, X., Zhu, H.H., Wang, J., Zhang, Q., Shi, B., Schenato, L., Pasuto, A., 2022. Subsurface multi-physical monitoring of a reservoir landslide with the fiber-optic nerve system. *Geophys. Res. Lett.* 49 (11), e2022GL098211.
- Yin, Y.P., Huang, B.L., Wang, W.P., Wei, Y.J., Ma, X.H., Ma, F., Zhao, C., 2016. Reservoir-induced landslides and risk control in three Gorges project on Yangtze River, China. *J. Rock Mech. Geotech. Eng.* 8, 577–595.
- Zeni, L., Picarelli, L., Avolio, B., Coscetta, A., Papa, R., Zeni, G., Di Maio, C., Vassallo, R., Minardo, A., 2015. Brillouin optical time-domain analysis for geotechnical monitoring. *J. Rock Mech. Geotech. Eng.* 7 (4), 458–462.
- Zhang, C.C., Shi, B., Zhang, S., Gu, K., Liu, S.P., Gong, X.L., Wei, G.Q., 2021a. Micro-anchored borehole fiber optics allows strain profiling of the shallow subsurface. *Sci. Rep.* 11, 9173.
- Zhang, C.Y., Yin, Y.P., Yan, H., Li, H.X., Dai, Z.W., Zhang, N., 2021b. Reactivation characteristics and hydrological inducing factors of a massive ancient landslide in the three Gorges Reservoir, China. *Eng. Geol.* 292, 106273.

- Zhang, L., Shi, B., Zhu, H.H., Yu, X.B., Han, H.M., Fan, X.D., 2021c. PSO-SVM-based deep displacement prediction of Majiagou landslide considering the deformation hysteresis effect. *Landslides* 18, 179–193.
- Zhang, L., Zhu, H.H., Han, H.M., Shi, B., 2023. Fiber optic monitoring of an anti-slide pile in a retrogressive landslide. *J. Rock Mech. Geotech. Eng.* <https://doi.org/10.1016/j.jrmge.2023.02.011>.
- Zhang, Y., Xue, Z.Q., 2019. Deformation-based monitoring of water migration in rocks using distributed fiber optic strain sensing: a laboratory study. *Water Resour. Res.* 55, 8368–8383.
- Zhu, H.H., Shi, B., Zhang, C.C., 2017. FBG-based monitoring of geohazards: current status and trends. *Sensors* 17 (3), 452.
- Zhu, H.H., 2023. Engineering geological interfaces: from multivariate characterization to evolution mechanism. *Bull. Geol. Sci. Technol.* 42 (1), 1–20 (in Chinese).
- Zscheischler, J., Westra, S., Van Den Hurk, B.J.J.M., Seneviratne, S.I., Ward, P.J., Pitman, A., et al., 2018. Future climate risk from compound events. *Nat. Clim. Change* 8 (6), 469–477.



Dr. Honghu Zhu is currently a Professor at the School of Earth Sciences and Engineering and the Dean of the Institute of Earth Exploration and Sensing, Nanjing University, China. He holds a Ph.D. degree in Geotechnical Engineering from the Hong Kong Polytechnic University. His research interests lie primarily in fiber optic monitoring and stability analysis of geoenvironment problems, with particular emphasis on interface behaviors. His research outputs have been transformed and applied in many projects, such as landslide monitoring in the Three Gorges Reservoir area, debris flow prevention and control in Wenchuan earthquake area, and structural health monitoring of the Pearl River Delta water conveyance tunnel. In the past decade, he has co-authored 2 books, 12 patents, and over 80 journal and conference papers. He is the recipient of the 1st-class Prize of National Scientific & Technological Progress Award of China of 2018. He served as an editorial board member of *Journal of Rock Mechanics and Geotechnical Engineering (JRMGE)* and *International Journal of Geosynthetics and Ground Engineering*.